Research Article

Changming Yang, Shiyu Qin, Yan Zuo, Yang Shi, Tong Bie, Ming Shao* and Yu Yu*

Waveguide Schottky photodetector with tunable barrier based on $Ti_3C_2T_x$/p-Si van der Waals heterojunction

https://doi.org/10.1515/nanoph-2021-0415
Received July 28, 2021; accepted October 2, 2021;
published online October 18, 2021

Abstract: MXene, a new advanced two-dimensional material, has attracted great attention in energy storage, transparent electrodes, and electromagnetic shielding due to its high conductivity, high specific surface area, and hydrophilic surface. Given the solution-processability and tunable work function, MXene also holds great potential for wide-range photodetection and integrated optics. Here, we demonstrate a waveguide integrated Schottky photodetector based on $Ti_3C_2T_x$/Si van der Waals heterojunction. Specifically, the barrier of the Schottky photodetector can be adjusted by using simple surface treatment. The work function of the $Ti_3C_2T_x$ is reduced from 4.66 to 4.43 eV after vacuum annealing, and the barrier height of $Ti_3C_2T_x$/p-Si Schottky junction is correspondingly increased from 0.64 to 0.72 eV, leading to 215 nm working wavelength blueshift. The photodetector exhibits working wavelength tunability in short-wavelength infrared regions due to the engineered Schottky barrier. To our best knowledge, this is the first demonstration of utilizing MXene in waveguide-integrated photodetection, showing the potential applications for various scenarios thanks to the flexible working wavelength range induced by the tunable barrier.

Keywords: 2D materials; MXene; $Ti_3C_2T_x$/p-Si; waveguide Schottky photodetectors.

Changming Yang and Shiyu Qin have contributed equally to this work.

***Corresponding authors: Ming Shao and Yu Yu**, Wuhan National Laboratory for Optoelectronics, Huazhong University of Science and Technology, 1037 Luoyu Road, Wuhan 430074, China,
E-mail: mingshao@hust.edu.cn (M. Shao), yuyu@mail.hust.edu.cn (Y. Yu). https://orcid.org/0000-0003-3709-7785 (M. Shao), https://orcid.org/0000-0002-8421-6794 (Y. Yu)
Changming Yang, Shiyu Qin, Yan Zuo, Yang Shi and Tong Bie, Wuhan National Laboratory for Optoelectronics and School of Optical and Electrical Information, Huazhong University of Science and Technology, Wuhan 430074, China

1 Introduction

MXenes are a new class of two-dimensional transition metal carbides, carbonitrides, and nitrides, which have drawn a great amount of interest due to their impressive electronic, optical, and mechanical properties [1–3]. Among the experimentally synthesized over 20 different MXenes, $Ti_3C_2T_x$ is the most studied one and thus better understood [4], where T represents the surface-terminated functional groups, such as –OH, –F, and =O. Owing to the high electrical conductivity, broadband nonlinear optical response, high photothermal conversion efficiency, large saturable absorption, good chemical stabilities, and environment friendly, the $Ti_3C_2T_x$ has been explored in many applications, such as transparent electrodes, electromagnetic interference shielding, photocatalysts, mode-locking lasers, and surface-enhanced Raman scattering [5–12].

Besides, the other promising characteristics of $Ti_3C_2T_x$, including hydrophilic surface, intense surface plasmon excitations in short-wavelength infrared (SWIR) regions, and tunable work function, make $Ti_3C_2T_x$ a potential candidate for on-chip photodetection. First, the hydrophilic surface allows $Ti_3C_2T_x$ to be easily transferred and grown by complementary metal-oxide-semiconductor compatible manufacturing processes [13–16]. Second, the real part of permittivity of $Ti_3C_2T_x$ becomes negative in SWIR regions, indicating the onset of free carrier oscillations [17]. Previous work has experimentally confirmed that surface plasmon polaritons could be excited in $Ti_3C_2T_x$ in SWIR regions by electron energy loss spectroscopic microscopy [18]. Third, the work function of $Ti_3C_2T_x$ can be adjusted using different synthetic methods or surface treatment methods [19, 20]. In contrast with graphene [21], the work function adjustment of $Ti_3C_2T_x$ is nonvolatile and wide-range, and it strongly depends on the surface-terminated function groups. Compared to a bare surface, the =O termination always increases the work function of MXenes, while –OH decreases it and –F has either trend depending on the specific material [22]. Since the Schottky barrier depends on the difference in the work function of the two materials in contact, a

flexible and suitable barrier height can be obtained by engineering the work function of $Ti_3C_2T_x$. Previous reports showed several MXene based photodetection applications, in which MXene is either used as electrodes [23, 24] or used to improve the responsivity of the detector by surface plasmon effect [25, 26]. However, there is no report on the wide response range tunable photodetector taking advantage of the modification work function of MXene, especially on the silicon photonic platform.

Here, an on-chip Schottky SWIR photodetector is constructed by forming MXene–Si van der Waals heterojunction. The $Ti_3C_2T_x$ is spray deposited onto the p-Si waveguide to form a good Schottky contact. We achieved 0.23 eV of the work function of $Ti_3C_2T_x$ adjustment by thermal annealing. The experimental results show that the measured responsivities at telecom wavelengths show a variation of an order of magnitude after thermal annealing. Moreover, the work function of the $Ti_3C_2T_x$ is reduced from 0.23 eV after vacuum annealing, leading to a 215 nm working wavelength blueshift. Consequently, the photodetector demonstrates wide working wavelength tunability in SWIR regions. Our work highlights that MXenes are prospective in on-chip optical communication, wide-spectrum photodetection, and on-chip optical sensing applications.

2 Results and discussion

2.1 Device structure and working principle

The proposed waveguide Schottky photodetector is schematically depicted in Figure 1a. It contains a p doping silicon waveguide with a ridge on one side, a $Ti_3C_2T_x$ film, and two gold electrodes. The grating couplers are used to coupler SWIR light into/out of the silicon waveguide, with fundamental quasi-transverse electric (TE_0) mode. When propagating to the region of the Schottky junction, the light is absorbed by $Ti_3C_2T_x$ and the photocurrent is produced under reversed bias. The p doping region is used to form a Schottky contact of low barrier height with $Ti_3C_2T_x$, while the p++ doping region is used to form an ohmic contact with the electrode. The whole silicon device is fabricated on a silicon-on-insulator (SOI) wafer with 2 μm buried oxide and 220 nm top silicon, through deep UV lithography. The cross-section of the proposed photodetector is shown in Figure 1b. In order to facilitate the transfer of MXene to the waveguide, the width of silicon waveguide W_1 is tapered from 500 nm to 10 μm through an adiabatic tapering process. The widths of p doping region W_2 and p++ doping region W_3 in the 90 nm-height slab layer are 20 and 10 μm, respectively. Firstly, we use a customized mask and UV lithography to transfer the required pattern to the photoresist, and then the synthesized MXene colloidal solution was sprayed onto the whole chip. Finally, acetone is used to remove the redundant photoresist and MXene to obtain the required MXene film with a feature size of 60 μm × 40 μm. The film thickness is measured to be 130 nm by step profiler and the length of the Schottky junction is 60 μm, ensuring the light being fully absorbed. The microscope image of the fabricated device is shown in Figure 1c.

The principle of the proposed waveguide Schottky photodetector is based on the internal photoemission (IPE) process [27]. The energy band diagram of the equilibrium state Schottky junction of $Ti_3C_2T_x$/p-Si heterostructure is shown in Figure 2a. According to a previous report, the Schottky barrier energy for the $Ti_3C_2T_x$/p-Si contact (Φ_B) is calculated by the following equation [28]:

$$\Phi_B = S[E_g - (W_m - \chi)] + B \tag{1}$$

where S and B are parameters depending on the distribution and density of the surface states. B is a constant, and the value of S varies from 0 to 1. The surface function groups like –OH, –F, and =O on the MXene easily form abundant surface states at the silicon layer, which is strongly influenced by the materials synthesis, film deposition, and post thermal annealing process. Thus, the change of work function value is not identical to the variation of the Schottky barrier height. W_m is the work function of the $Ti_3C_2T_x$, χ is the electron affinity of silicon, and E_g is the bandgap of silicon. The obtained Schottky barrier is usually lower than the bandgap of silicon, allowing IPE of holes from $Ti_3C_2T_x$ to p-silicon upon the absorption of infrared photons with energy $h\nu$ exceeding the barrier at the interface. The IPE process can be divided into three steps: photoexcitation, transport, and emission. Firstly, an electron in a state below W_m absorbs the energy of an incident photon in the silicon waveguide, raising it to a state above W_m. Correspondingly, a hot hole is raised from a state above W_m to a state below W_m (photoexcitation step). Then the hot hole is headed toward the interface (transport step). If the hot hole gains sufficient energy to overcome the barrier, it can be emitted into the silicon and finally collected as photocurrent (emission step). In the ideal case, as the electron affinity of silicon χ and the bandgap of silicon E_g remain constant, the barrier Φ_B depends on the work function W_m. Meanwhile, the Φ_B determines the internal quantum efficiency and the cutoff wavelength of the Schottky photodetector [29]. The responsivity R of Schottky photodetector can be expressed by

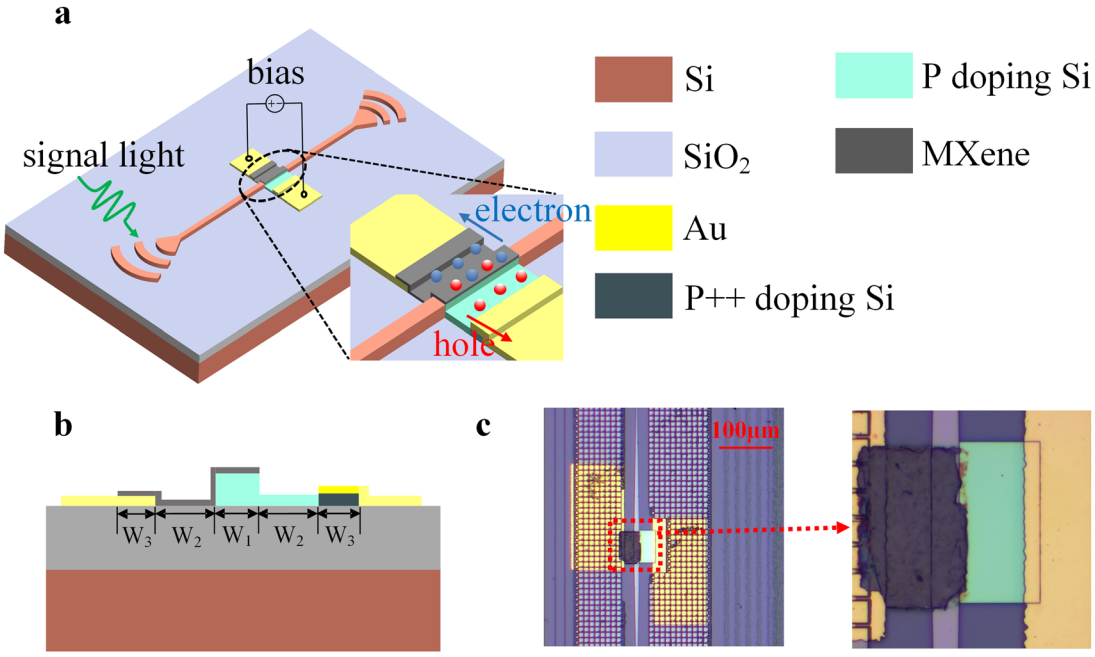

Figure 1: Structures of proposed waveguide Schottky photodetector.
(a) The whole structure is based on an SOI chip with a p doping silicon rib waveguide. The $Ti_3C_2T_x$ film is deposited on the side of the doped waveguide without a ridge layer and covers the whole doped silicon waveguide and part of the gold electrode. (b) The cross-section of the proposed photodetector. (c) Microscope image of the proposed photodetector.

$$R = \frac{qA}{2h\nu}\left(1 - \sqrt{\frac{\Phi_B}{h\nu}}\right)^2 \tag{2}$$

where q is the elemental charge, h is Planck's constant, ν is the frequency of incident photons, and A is the optical absorptance. Using the equation, we can get the ideal responsivity curve under the different barrier Φ_B, as depicted in Figure 2b. As Φ_B increases, the overall responsivity decreases and the cutoff wavelength is blue-shifted. According to Equation (1), the Schottky barrier between MXene and Si will be modified, depending on the work function of MXene. Actually, the computed result in Figure 2b is calculated by Equation (2) under the ideal case that the external quantum efficiency is 100%, and some issues including surface states are not taken into consideration. Therefore, the computed responsivities in Figure 2b are much larger than the responsivities of the actual device. Recent studies show that the work function of synthesized $Ti_3C_2T_x$ can be effectively changed by modifying the surface termination moieties such as –OH, –F, and =O, through thermal annealing [30]. Therefore, thermal annealing is employed to adjust the Schottky barrier of $Ti_3C_2T_x$/p-Si.

2.2 Electrical characterizations of the tunable barrier

Since $Ti_3C_2T_x$ shows the metallic electrical conductivity and tunable work function, we first check the change of the work function of $Ti_3C_2T_x$ under thermal annealing post treatment. The $Ti_3C_2T_x$ film is spray deposited on the SOI substrate in a large area, followed by the vacuum thermal annealing in a tube furnace at 300 °C for 2 h. As depicted in Figure 3, the Kelvin probe is used to measure the work functions at different positions of $Ti_3C_2T_x$ film. We measured the work functions of 100 different positions of the $Ti_3C_2T_x$ film before and after annealing. From the average value of the work functions at different positions, the work function of the $Ti_3C_2T_x$ film is shifted from 4.66 to 4.43 eV after the annealing treatment. The decreased work function is probably due to the removing –F, and =O functional groups with high dipole moment by the vacuum annealing, as pointed out by the theoretical predictions and previous experiment results [31, 32].

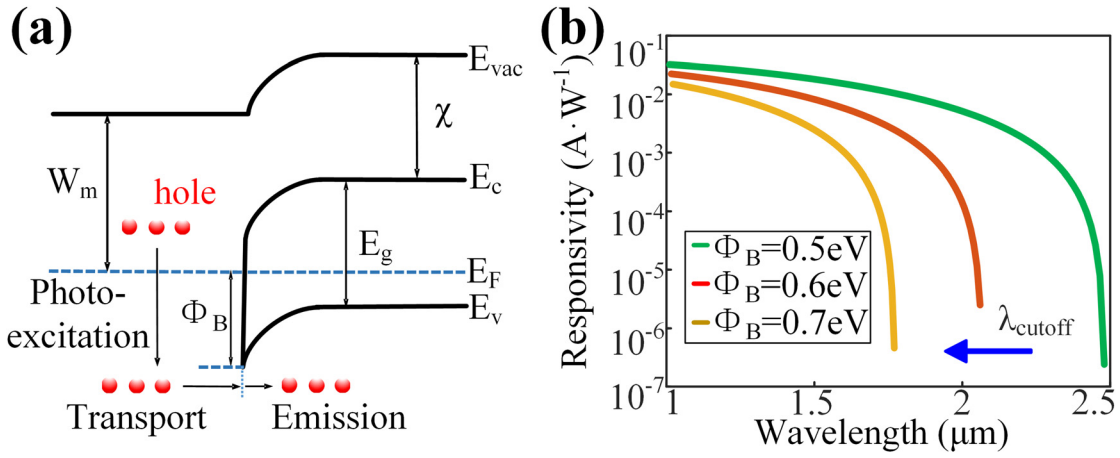

Figure 2: (a) The energy band diagram of the $Ti_3C_2T_x$/p-Si Schottky junction upon illumination. Here, E_{vac}, E_c, and E_v stand for the vacuum level, the bottom of the conduction band, and the top of the valence band, respectively. E_F corresponds to the Fermi energy in the silicon at thermal equilibrium. Φ_B is the barrier height between $Ti_3C_2T_x$ and p-Si, W_m is the work function of $Ti_3C_2T_x$, χ is the electron affinity of p-Si, and E_g is the bandgap of p-Si. (b) The computed responsivity of the ideal $Ti_3C_2T_x$/p-Si Schottky photodetector with a different barrier Φ_B.

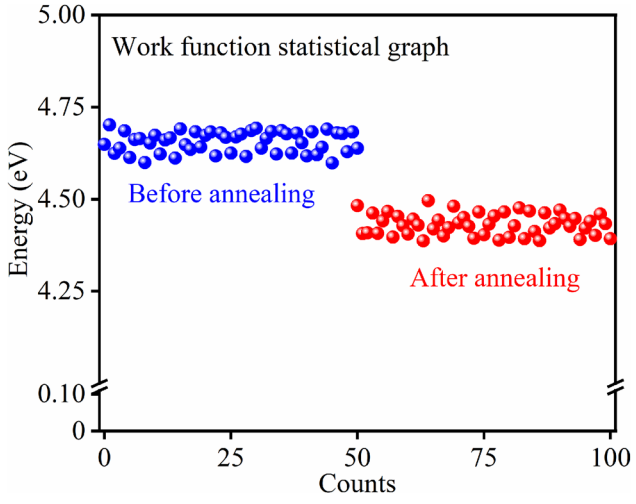

Figure 3: Work functions at different positions of $Ti_3C_2T_x$ film.

Next, we measured the current–voltage curves of $Ti_3C_2T_x$/p-Si heterostructure under different temperatures. As depicted in Figure 4a, both forward and reversed currents are increased with temperature, which is consistent with the predication from a Schottky junction obeying the thermionic emission model [33]. As most practical Schottky diodes show deviations from ideal thermionic emission behavior, the current–voltage relationship can be expressed as

$$I = I_s\left[\frac{\exp(qV_D)}{nkT} - 1\right] \tag{3}$$

where n is the ideality factor, q is the elemental charge, V_D is the voltage applied across the diode, k is the Boltzmann constant and T is the absolute temperature. The ideal factor of the diode is a key parameter to measure the quality of the Schottky junction. The closer it is to 1, the better the Schottky junction performance of the $Ti_3C_2T_x$/p-Si device. I_s can be expressed by

$$I_s = A_{\text{eff}}A^*T^2\exp\left(-\frac{q\Phi_B}{kT}\right) \tag{4}$$

where A_{eff} is the effective area of the Schottky diode, A^* is the Richardson constant and it is 32 A cm^{-2} K^{-2} for p-Si substrates. Using the current–voltage data, the ideal factors and Schottky barriers height of the Schottky contact can be easily extracted by exploiting the modified Norde method [34]. Accordingly, the tunable barrier is tested by measuring the current–voltage characteristics of the proposed photodetector before and after vacuum annealing at 300 °C for 2 h. As shown in Figure 4b, the dark current after the annealing treatment is overall reduced. According to the fitting method, the ideal factors and Schottky barriers height before and after annealing are 3.1/0.64 eV and 2.6/0.72 eV, respectively, at 20 °C. The decreased current and ideal factor after annealing imply that the defect of $Ti_3C_2T_x$ and p-Si interface is removed and the Schottky junction performance becomes better, and the increased barrier height implies that the barrier of $Ti_3C_2T_x$/p-Si Schottky junction can be adjusted by annealing.

2.3 Optical characterizations of the tunable barrier

Since the barrier determines the internal quantum efficiency of the Schottky photodetector, we further verify the

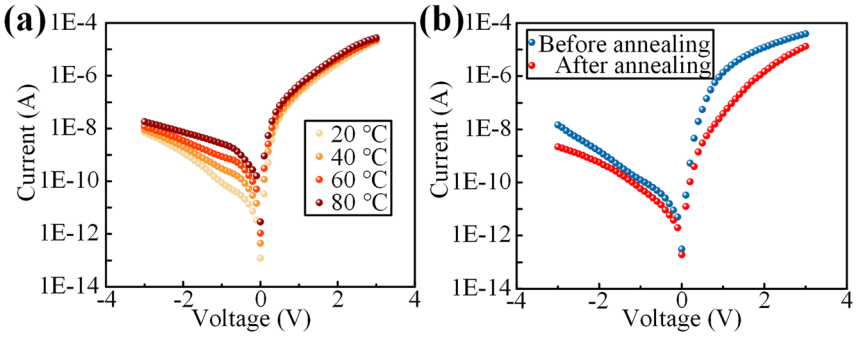

Figure 4: (a) The temperature-dependent current–voltage measurements of $Ti_3C_2T_x$/p-Si Schottky junction in the dark. (b) The current–voltage characteristics of the Schottky photodetector in the dark before and after vacuum annealing.

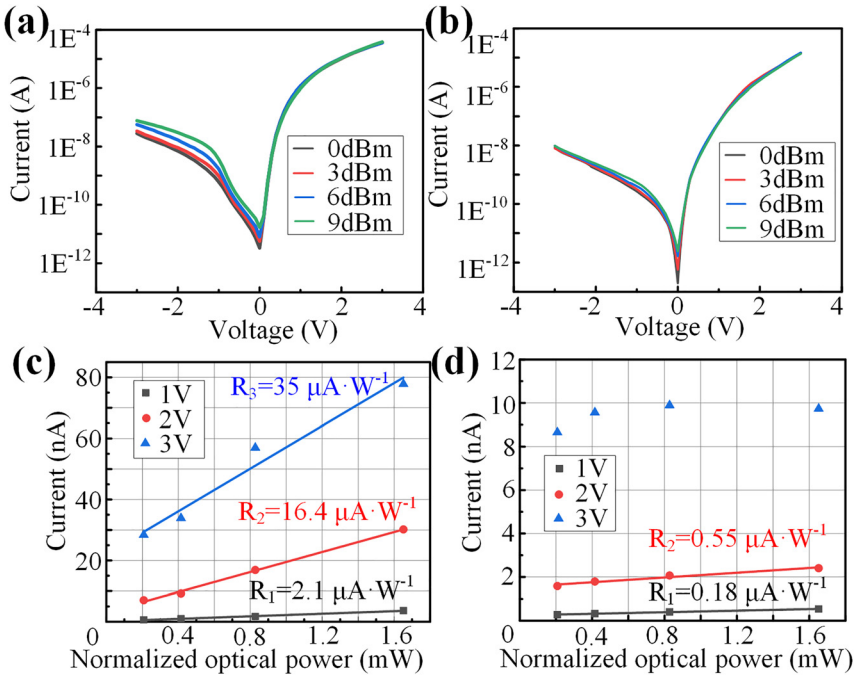

Figure 5: Current–voltage measurements under 1550 nm illumination (a) before and (b) after vacuum annealing. And photocurrent as a function of the optical power at different reversed biases (c) before and (d) after vacuum annealing.

tunability of the barrier from the responsivity test. In order to calculate the responsivity accurately, the loss spectrum of the grating coupler is first characterized by an optical spectrum analyzer (AQ6370, Yokogawa, Japan), and it is used to normalize the input optical power of different wavelengths. Compared with the absorption of MXene, the absorption of the p-doping Si with a low doping concentration is very weak in the wavelength range from 1530 to 1570 nm. Therefore, we exclude the absorption of p doping Si. Due to the bandwidth limitation of the grating coupler, we measure the photocurrent of the photodetector at five wavelengths by a sourcemeter (2634B, Keithley, USA), equally spaced from 1530 to 1570 nm. Figure 5a and b show the measured current-voltage characteristics of the photodetector upon 1550 nm light illumination, before and after vacuum annealing. The photocurrent increases with the increase of input optical power, and the increment of photocurrent after vacuum annealing is significantly smaller. In other words, the Schottky barrier height after annealing is higher, leading to a decrease in the responsivity of the photodetector. To obtain the responsivities, we plot the photocurrent values at the reversed bias of 1, 2, and 3 V as a

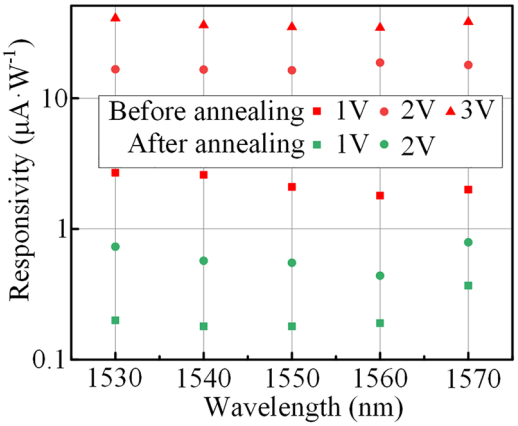

Figure 6: Comparison of responsivity before and after vacuum annealing at five operation wavelengths.

function of normalized optical power, as shown in Figure 5c and d. The responsivities of photodetector without thermal annealing are 2.1, 16.4, and 35 μA W^{-1} for 1, 2, and 3 V, respectively. After vacuum annealing, the responsivities at the reversed bias of 1 and 2 V are 0.18 and 0.55 μA W^{-1}, respectively. Due to the low on/off ratio at the high reversed bias, the responsivity at the reversed bias of 3 V is hard to be measured.

Furthermore, the responsivities at the other four wavelengths are also measured, as shown in Figure 6. The red mark and the green mark indicate the responsivity values obtained before and after thermal annealing. However, since the input optical power in the waveguide is partially scattered into the air or the substrate when entering the Schottky junction area, the actual responsivity of the photodetector may be even higher. As the barrier height of the $Ti_3C_2T_x$/p-Si Schottky junction is shifted from 0.64 to 0.72 eV after thermal annealing, the measured responsivities at telecom wavelengths show a variation of an order of magnitude, which is consistent with the theoretical expectation.

2.4 Discussion

The results above indicate that the barrier of the proposed waveguide integrated $Ti_3C_2T_x$/p-Si Schottky photodetector can be modified by adjusting the functional group of $Ti_3C_2T_x$ through vacuum annealing. Though the responsivity of the demonstrated photodetector is ~40 μA W^{-1}, some effective methods can be utilized to improve its performance. Firstly, exciting the surface plasmons of the $Ti_3C_2T_x$/Si interface is a feasible method to improve the internal quantum efficiency and responsivity, such as doping gold particles in the MXene film. The hot electrons or holes in the MXene film typically acquire low transmission probability due to considerable momentum mismatch and poor overlap of the electron wavefunctions between MXene and silicon. Therefore, exciting the surface plasmons is a common way to enhance light absorption and increase the transmission probability of hot carriers by concentrating optical electromagnetic energy at the boundary. On the other hand, adopting other grow methods such as chemical vapor deposition or using other kinds of MXene such as Mo_2CT_x to construct a planar and compact film is also a promising way. Due to the fabrication limitation, the synthesized $Ti_3C_2T_x$ contains clastic films of different sizes and the film grown by spray coating is unfavorable for hot carriers to transit into silicon. It can be expected to achieve a high responsivity and wide-range tunable barrier by applying these methods in future work.

3 Conclusions

In summary, we propose and demonstrate a waveguide integrated $Ti_3C_2T_x$/p-Si Schottky photodetector with a tunable barrier by modifying the work function of $Ti_3C_2T_x$. Using the vacuum annealing method, the work function of $Ti_3C_2T_x$ film can be shifted from 4.66 to 4.32 eV. Correspondingly, the barrier of $Ti_3C_2T_x$/p-Si Schottky photodetector is adjusted from 0.64 to 0.72 eV, leading to a 215 nm blue-shift of working wavelength. The measured responsivities at telecom wavelengths show a variation, which further validates the increased barrier. This work brings MXene to waveguide-integrated photodetection fields and shows the potential applications for various scenarios thanks to the flexible working wavelength range induced by the tunable barrier.

Author contributions: All the authors have accepted responsibility for the entire content of this submitted manuscript and approved submission.
Research funding: This work is funded by the National Key Research and Development Program of China (2019YFB1803801), National Natural Science Foundation of China (61775073, 61922034), Key Research and Development Program of Hubei Province (2020BAA011), and program for HUST Academic Frontier Youth Team (2018QYTD08).
Conflict of interest statement: The authors declare no conflicts of interest regarding this article.

References

[1] B. Anasori, M. R. Lukatskaya, and Y. Gogotsi, "2D metal carbides and nitrides (MXenes) for energy storage," *Nat. Rev. Mater.*, vol. 2, p. 16098, 2017.
[2] M. Naguib, V. N. Mochalin, M. W. Barsoum, and Y. Gogotsi, "25th Anniversary article: MXenes: a new family of two-dimensional materials," *Adv. Mater.*, vol. 26, p. 992, 2014.
[3] J. Yi, J. Li, S. Huang, et al., "Ti_2CT_x MXene-based all-optical modulator," *InfoMat*, vol. 2, pp. 601–609, 2019.
[4] M. Naguib, M. Kurtoglu, V. Presser, et al., "Two-dimensional nanocrystals produced by exfoliation of Ti_3AlC_2," *Adv. Mater.*, vol. 23, pp. 4248–4253, 2011.
[5] J. Halim, M. R. Lukatskaya, K. M. Cook, et al., "Transparent conductive two-dimensional titanium carbide epitaxial thin films," *Chem. Mater.*, vol. 26, pp. 2374–2381, 2014.
[6] F. Shahzad, M. Alhabeb, C. B. Hatter, et al., "Electromagnetic interference shielding with 2D transition metal carbides (MXenes)," *Science*, vol. 353, p. 1137, 2016.
[7] Y. Zuo, Y. Gao, S. Qin, et al., "Broadband multi-wavelength optical sensing based on photothermal effect of 2D MXene films," *Nanophotonics*, vol. 9, pp. 123–131, 2020.
[8] Y. I. Jhon, J. Koo, B. Anasori, et al., "Metallic MXene saturable absorber for femtosecond mode-locked lasers," *Adv. Mater.*, vol. 29, 2017, https://doi.org/10.1002/adma.201702496.

[9] H. Wang, R. Peng, Z. D. Hood, M. Naguib, S. P. Adhikari, and Z. Wu, "Titania composites with 2DTransition metal carbides as photocatalysts for hydrogen production under visible-light irradiation," *ChemSusChem*, vol. 9, pp. 1490–1497, 2016.
[10] E. Satheeshkumar, T. Makaryan, A. Melikyan, H. Minassian, Y. Gogotsi, and M. Yoshimura, "One-step solution processing of Ag, Au and Pd@MXene hybrids for SERS," *Sci. Rep.*, vol. 6, p. 32049, 2016.
[11] L. Liu and T. Zhai, "Wafer-scale vertical van der Waals heterostructures," *InfoMat*, vol. 3, pp. 3–21, 2020.
[12] X. Zhou, X. Hu, S. Zhou, et al., "Tunneling diode based on WSe_2/SnS_2 heterostructure incorporating high detectivity and responsivity," *Adv. Mater.*, vol. 30, 2018, https://doi.org/10.1002/adma.201703286.
[13] K. Hantanasirisakul, M.-Q. Zhao, P. Urbankowski, et al., "Fabrication of $Ti_3C_2T_x$ MXene transparent thin films with tunable optoelectronic properties," *Adv. Electron. Mater.*, vol. 2, p. 1600050, 2016.
[14] N. Kurra, B. Ahmed, Y. Gogotsi, and H. N. Alshareef, "MXene-on-paper coplanar microsupercapacitors," *Adv. Energy Mater.*, vol. 6, p. 1601372, 2016.
[15] M. Alhabeb, K. Maleski, B. Anasori, et al., "Guidelines for synthesis and processing of two-dimensional titanium carbide ($Ti_3C_2T_x$ MXene)," *Chem. Mater.*, vol. 29, pp. 7633–7644, 2017.
[16] X. Jiang, W. Li, T. Hai, et al., "Inkjet-printed MXene micro-scale devices for integrated broadband ultrafast photonics," *NPJ 2D Mater. Appl.*, vol. 3, p. 34, 2019.
[17] A. D. Dillon, M. J. Ghidiu, A. L. Krick, et al., "Highly conductive optical quality solution-processed films of 2D titanium carbide," *Adv. Funct. Mater.*, vol. 26, pp. 4162–4168, 2016.
[18] V. Mauchamp, M. Bugnet, E. P. Bellido, et al., "Enhanced and tunable surface plasmons in two-dimensional Ti_3C_2 stacks: electronic structure versus boundary effects," *Phys. Rev. B*, vol. 89, 2014, https://doi.org/10.1103/physrevb.89.235428.
[19] H.-W. Wang, M. Naguib, K. Page, D. J. Wesolowski, and Y. Gogotsi, "Resolving the structure of $Ti_3C_2T_x$ MXenes through multilevel structural modeling of the atomic pair distribution function," *Chem. Mater.*, vol. 28, pp. 349–359, 2016.
[20] I. Persson, L.-Å. Näslund, J. Halim, et al., "On the organization and thermal behavior of functional groups on Ti_3C_2 MXene surfaces in vacuum," *2D Mater.*, vol. 5, p. 015002, 2017.
[21] X. Li and H. Zhu, "The graphene-semiconductor Schottky junction," *Phys. Today*, vol. 69, pp. 46–51, 2016.
[22] Y. Liu, H. Xiao, and W. A. Goddard, III, "Schottky-barrier-free contacts with two-dimensional semiconductors by surface-engineered MXenes," *J. Am. Chem. Soc.*, vol. 138, pp. 15853–15856, 2016.
[23] Z. Kang, Y. Ma, X. Tan, et al., "MXene–silicon van der Waals heterostructures for high-speed self-driven photodetectors," *Adv. Electron. Mater.*, vol. 3, p. 1700165, 2017.
[24] K. Montazeri, M. Currie, L. Verger, P. Dianat, M. W. Barsoum, and B. Nabet, "Mxene photodetectors: beyond gold: spin-coated Ti_3C_2-based MXene photodetectors (Adv. Mater. 43/2019)," *Adv. Mater.*, vol. 31, p. 1970307, 2019.
[25] Y. Dong, S. Chertopalov, K. Maleski, et al., "Saturable absorption in 2D Ti_3C_2 MXene thin films for passive photonic diodes," *Adv. Mater.*, vol. 30, p. 1705714, 2018.
[26] Y. Yang, J. Jeon, J.-H. Park, et al., "Plasmonic transition metal carbide electrodes for high-performance InSe photodetectors," *ACS Nano*, vol. 13, pp. 8804–8810, 2019.
[27] J. S. Helman and F. Sánchez-Sinencio, "Theory of internal photoemission," *Phys. Rev. B*, vol. 7, pp. 3702–3706, 1973.
[28] K. K. Chin, R. Cao, T. Kendelewicz, et al., "Transition from Schottky limit to bardeen limit in the Schottky barrier formation of al on n- and p-GaAs(110) interfaces," *MRS Online Proc. Libr.*, vol. 77, pp. 297–303, 1986.
[29] C. Scales and P. Berini, "Thin-film Schottky barrier photodetector models," *IEEE J. Quant. Electron.*, vol. 46, pp. 633–643, 2010.
[30] J. L. Hart, K. Hantanasirisakul, A. C. Lang, et al., "Control of MXenes' electronic properties through termination and intercalation," *Nat. Commun.*, vol. 10, p. 522, 2019.
[31] T. Schultz, N. C. Frey, K. Hantanasirisakul, et al., "Surface termination dependent work function and electronic properties of $Ti_3C_2T_x$ MXene," *Chem. Mater.*, vol. 31, pp. 6590–6597, 2019.
[32] H. A. Tahini, X. Tan, and S. C. Smith, "The origin of low workfunctions in OH terminated MXenes," *Nanoscale*, vol. 9, pp. 7016–7020, 2017.
[33] J.-P. Colinge and C. A. Colinge, *Physics of Semiconductor Devices*, New York, NY, USA, Springer Science & Business Media, 2005.
[34] S. K. Cheung and N. W. Cheung, "Extraction of Schottky diode parameters from forward current–voltage characteristics," *Appl. Phys. Lett.*, vol. 49, pp. 85–87, 1986.